Optical manipulation of metal-silica hybrid nanoparticles

Rodney R. Agayan[*a,b], Thomas Horvath[b], Brandon H. McNaughton[a,b], Jeffrey N. Anker[a,b], Raoul Kopelman[a,b]
[a]Appl. Physics Program, Univ. of Michigan, 2071 Randall Laboratory, Ann Arbor, MI 48109-1120
[b]Dept. of Chemistry, Univ. of Michigan, 930 North University, Ann Arbor, MI 48109-1055

ABSTRACT

Metallic nanoparticles are known to experience enhanced optical trap strengths compared to dielectric particles due to the increased optical volume, or polarizability. In our experience, larger metallic particles (~μm) are not easily trapped because momentum effects due to reflection become significant. Hybrid particles comprised of both metal and dielectric materials can circumvent this limitation while still utilizing a larger polarizability. Heterogeneous nanosystems were fabricated by embedding/coating silica nanoparticles with gold or silver in varying amounts and distributions. These compound particles were manipulated via optical tweezers, and their trapping characteristics quantitatively and qualitatively compared to homogeneous particles of comparable size. The parameters explored include the dependence of the trapping force on the percentage of loading of gold, the size of the embedded colloids, and the distribution of metal within the surrounding matrix or on its surface.

Keywords: nanoparticle, silica, metal, colloid, polarizability, laser tweezers, microscopy, trap stiffness

1. INTRODUCTION

In this work, optical tweezers are used to manipulate metal-silica hybrid nanoparticles with prospects of measuring light-matter interactions. A surge of advances in recent years[1-4] has made optical tweezers a promising technique for motion control of mesoscopic systems in physics, chemistry, and biology. Much of the progress has focused on modification of the laser beam configuration to enable multiple trap positions via time-sharing,[5] beamsplitting,[6] using diffractive optical elements,[7] or using spatial light modulators.[8] Other schemes utilize beams with spin or angular momentum, such as circularly polarized light and Laguerre-Gaussian beams, or rotated asymmetric beam patterns to generate torque on the trapped particle.[1-3] Much less work has been done concerning modification of the trapped particle itself, nonetheless some developments worth mentioning include schemes for trapping metals,[1] the optical tweezing of nonspherical particles,[9] the optical fabrication and tweezing of a light-driven turbine,[10] and the optical tweezing of core-shell colloidal systems.[11]

There is growing interest in the use of hybrid nanosystems such as core-shell colloidal systems outside the field of optical tweezing. Single-nanoparticle surface-enhanced Raman scattering (SERS) has been observed using heterogeneous systems comprised of compound dielectric-metal[12] and dielectric-semiconductor materials.[13] The effects of localized surface plasmon resonances which enable such enhanced optical properties have been studied for optically trapped metal nanoparticles,[14-16] however little has been done on optically trapped hybrid systems. Another application of hybrid nanoparticles is in subcellular magnetic resonance imaging[17] and chemical imaging with biosensing probes.[18] In particular, fiber-based silica-gold-fluorophore systems have been used as selective nitric-oxide sensors.[19-21] Also, nanosystems consisting of dielectric particles half-coated with metal have been fabricated to allow sensing with increased signal-to-background ratios and for microrheological studies.[22,23] Nanoparticle versions of these biosensors combined with optical tweezing can provide a non-invasive means of intracellular investigation.

[*] ragayan@umich.edu, horvatht@umich.edu, bmcnaugh@umich.edu, janker@umich.edu, kopelman@umich.edu; for all authors phone 1 734 764-7541; fax 1 734 936-2778; http://www.umich.edu/~koplab

Optical Trapping and Optical Micromanipulation, edited by Kishan Dholakia, Gabriel C. Spalding, Proceedings of SPIE Vol. 5514 (SPIE, Bellingham, WA, 2004) · 0277-786X/04/$15 doi: 10.1117/12.559757

In this paper, we consider the optical tweezing of dielectric-metal core-shell and core-half-shell nanoparticles. To investigate the trapping of our hybrid particles, we observed their position fluctuation dynamics while held in our optical tweezers. By comparing trap stiffness among all particle types, we gain information on the light-particle interactions strengths. Further image analysis provides qualitative effects of asphericity on laser trapping stability.

2. THEORY

The most appropriate theoretical description of neutral particle trapping using single-beam gradient optical tweezers depends on the particle size relative to the wavelength of the trapping beam. For particle diameters much smaller than the wavelength ($d << \lambda$), the particle, described in the Rayleigh regime, is treated as a simple, induced dipole oscillating in a harmonic electric field.[24,25] In this regime, trapping forces can be resolved into two components:[26] a scattering component, in the direction of the incident light, and a gradient component, along the intensity gradient. Stable trapping for a single-beam gradient trap occurs when the gradient force exceeds the scattering force to generate a potential well deeper than the particle's thermal energy due to Brownian motion. It is believed that the scattering force on a nonabsorbing Rayleigh particle is proportional to its scattering cross section, so the scattering force scales with the square of the polarizability (volume),[27,28] or as d^6. The gradient force scales linearly with polarizability (volume),[27,29] thus having a d^3 dependence. These quadratic and linear dependences on polarizability for the scattering and gradient forces, respectively, suggest that stable three-dimensional single-beam trapping occurs only for particles smaller than some maximum threshold size. Svoboda and Block[30] use this polarizability dependence to explain increased trapping forces for gold Rayleigh particles over latex particles of similar size surrounded by water. Their analysis contends that 40 nm gold particles are the maximum size for stable three-dimensional trapping.

For particles with diameters much larger than the trapping wavelength ($d >> \lambda$), conventional theory assumes the geometrical optics regime in which trapping forces can be attributed to momentum exchange due to the refraction and reflection of plane waves.[1,31] In this size regime, dielectric particles are readily trapped in three dimensions whereas metallic particles are difficult to trap three-dimensionally because scattering, reflection, and absorption are increased.

To quantify trap strength, one can analyze the particle's position behavior as the particle falls in the trap,[32,33] while the trap is moved relative to the surrounding medium,[32,34-36] or as the particle experiences dynamic position fluctuations due to Brownian motion in a stationary trap.[30,34,37-39] The last method, which we utilize in the current work, assumes a particle surrounded by a medium of viscosity η trapped in a harmonic potential well subject to a microscopic random thermal force. The small Reynolds numbers of practical systems indicate that viscous forces dominate over inertial forces,[37] thus the particle's motion can be described by the reduced Langevin equation:

$$\gamma\dot{x} + \kappa x = F(t), \tag{1}$$

where x and $\dot{x}$ are the particle position and velocity, respectively, γ is the hydrodynamic drag coefficient equal to $3\pi\eta d$, and κ is the trap stiffness or harmonic force spring constant. Fourier domain solutions of this system are well known and deviations often present in experiment have been studied in great detail.[37,38,40,41] One finds that the power spectral density (PSD) of the position fluctuations follows a Lorentzian profile:

$$S(f) = S_0 \frac{f_c^2}{f_c^2 + f^2}, \tag{2}$$

with low-frequency PSD amplitude $S_0 = 4\gamma k_B T / \kappa^2$ and corner frequency $f_c = \kappa / 2\pi\gamma$, where k_B is Boltzmann's constant and T is absolute temperature. Note, for a given solvent, the corner frequency is proportional to the trap stiffness. If the particle is isotropic and trapped stably in three dimensions, the gradient force dominates the scattering force and is given by[24]

$$\left\langle F_g \right\rangle = \frac{\varepsilon_0}{4} \mathrm{Re}[\chi] \nabla \left(|E|^2 \right), \tag{3}$$

where ε_0 is the vacuum electric permittivity, χ is the particle susceptibility (or polarizability for Rayleigh particles) and E^2 is proportional to the laser beam power. Equating this to a harmonic restoring force $-\kappa x$, we see that if the gradient force dependence on laser power is linear, the corner frequency will also be proportional to laser power.

If a trapped particle remains close to the minimum of the potential well created by the laser beam, a harmonic potential is expected. The positions visited by the particle will then be Boltzmann-distributed as given below:

$$N(x) = N_0 \exp\left(-\frac{\kappa x^2}{2 k_B T} \right). \tag{4}$$

Our core-shell hybrid nanosystems consist of particles considered in the Rayleigh regime or the geometrical optics regime individually. Precise electromagnetic theory has not been found in the literature to describe such systems; however, some effects are expected. As the shell layer contains 40 nm metal Rayleigh colloids, the total polarizability of the system will be increased compared to pure silica while reflection is decreased compared to pure metal, potentially increasing trap strength. Since the metal colloids likely provide a small perturbation bound to a macroscopic 1 μm silica particle, position fluctuations for the system should follow macroscopic behavior with adjustments due to increased scattering and absorption, and due to induced material anisotropy. For our half-shell hybrid nanoparticles, the layer thickness is kept below the skin depth; therefore, reflection is again reduced. The material anisotropy is more severe, and, consequently, more drastic changes in trapping behavior are expected.

3. MATERIALS AND METHODS

To investigate the effects of metal composition on hybrid-particle optical trapping, various particle configurations were fabricated and characterized. Single particles from each sample were then optically trapped, and their motion dynamics recorded. The data was then analyzed to gain qualitative and quantitative information about the trap's properties.

3.1. Sample preparation

All of our sample particle-systems comprised a spherical dielectric core surrounded by an outer layer or shell of metal. The core consisted of commercially available silica microspheres while the outer shell is incorporated either by attaching gold or silver colloids, or via evaporation.

3.1.1. Aminated silica cores

A total of 212 mg of 0.97 μm diameter dry silica microspheres (Bangs Labs, Fishers, Indiana) were suspended in 40 mL of ethanol (99.5%, A.C.S. reagent grade, absolute, 200 proof) in a 100 mL round bottom flask. In order to provide amine groups to the surface of the silica, 1 mL of 3-aminopropyltriethoxysilane (99%, Aldrich, St. Louis, Montana) was added to the suspension. Amine functionalization of the silica particles is known to facilitate synthesis of silica-noble metal core-shell microspheres.[42] The reaction was allowed to run for 2 hours and 15 minutes in the sealed 100 mL round bottom flask with constant magnetic stirring to provide even distribution of the amine functionalization to the silica particles. The particles were filtered using a 0.8 μm ATTP Isopore™ Membrane filter (Millipore, Billerica, Massachusetts). They were re-suspended in ethanol to wash off any unreacted material and then filtered again. The particles were suspended in 10 mL of MilliQ de-ionized water for use.

3.1.2. Silica-gold core-shell microspheres

1 mL of a 5 nm diameter gold colloid (Ted Pella, Inc., Redding, California) suspension was added to a 20 mL scintillation vial. Because the colloid is certified to have been washed of all reactants during synthesis, citrate must be added to enable attachment of the colloids to the amine groups on the silica microspheres.[42] A 1 mL aliquot of 34 mM

sodium citrate solution (99%, A.C.S. reagent grade, Alfa Aesar, Ward Hill, Massachusetts) was added in order that the citrate ion would ligate the 5 nm gold colloid. After mixing, 1 mL of the amine functionalized silica microspheres was added to the scintillation vial. The mixture color changed from light red to deep red. The suspension was sonicated to re-suspend dark red particles that may have settled out of solution. After sonication, the suspension was centrifuged at 5000 rpm for 10 minutes. All of the particles at the bottom of the centrifuge tube, post-sonication, were deep-red in color while the solution was clear suggesting little unattached gold colloid had suspended. The clear solution was removed using a Pasteur pipette, and the particles were re-suspended in 10 mL of ethanol. Centrifugation and re-suspension in ethanol was repeated once more. The particles were filtered with the 0.8 μm ATTP Isopore™ filter until dry and re-suspended in 10 mL of de-ionized water for use.

For silica-gold core-shell particles containing larger gold colloids, a similar fabrication procedure was performed with the initial volumes being 0.100 mL of the amine functionalized silica combined with 1.00 mL of the 34 mM sodium citrate solution. A 10 mL aliquot of 40.3 nm diameter gold colloids (Ted Pella) was added, and the suspension was placed in an ultrasonic bath for 90 minutes. Upon removal from the bath, dark red particles quickly began to settle.

3.1.3. Silica-silver core-shell microspheres

Silver colloids of <5 nm diameter were synthesized according to the method described in the literature.[43] A 100 mL round bottom flask was cleaned with Alconox (White Plains, New York), rinsed, and dried thoroughly. After drying, 47.5 mL of MilliQ de-ionized water was added. The de-ionized water was de-oxygenated by bubbling with nitrogen gas for 30 minutes. Subsequent reactions all took place under vigorous stirring (1200 rpm).

After de-oxygenation, a 0.500 mL aliquot of 30 mM sodium citrate was added to the water and allowed to mix for several seconds. Next, 1.00 mL of 5 mM silver nitrate solution (EM Science, Gibbstown, New Jersey) was added to the mixture and allowed to mix for several seconds. After 0.500 mL of 50 mM sodium borohydride solution (99%, Aldrich) was added, the solution immediately turned a pale yellow color. The solution was then stirred for 30 seconds more before adding 0.500 mg/mL of poly(vinyl)pyrrolidone (M_w = 55,000 g/mol, Aldrich). The suspension turned dark yellow in color and was stirred an additional 30 minutes.

A 1 mL aliquot of the <5 nm silver colloid suspension was added to a scintillation vial, along with 1 mL of de-ionized water. The 34 mM sodium citrate was not needed (as in the preparation of silica-gold samples) because the citrate ion was still present from the colloid synthesis. 1 mL of the amine functionalized silica microspheres was added to the colloid suspension, immediately making the solution cloudy. Over time, all of the silica-silver core-shell particles came out of suspension and collected on the bottom of the scintillation vial. This mixture was filtered using the 0.8 μm ATTP Isopore™ filter. The particles were washed with several ethanol rinses, and dry particles were re-suspended in 10 mL of de-ionized water for experiments.

Again, silica-silver core-shell particles containing larger silver colloids were also fabricated with a similar procedure. Starting volumes were 0.100 mL of the amine functionalized silica and 1.00 mL of the 34 mM sodium citrate solution. 10 mL of 40 ± 5 nm silver colloids (Ted Pella) were added, and the suspension was sonicated. After sonication, yellow particles started to settle.

3.1.4. Silica-metal core-half-shell microspheres

MOONs (MOdulated Optical Nanoprobes) can be fabricated by coating one hemisphere of nanoparticles with an opaque metal as illustrated in Figure 1. Our procedure utilizes commercially available silica nano- and microspheres (Bang's Labs) in combination with a gold sputter chamber.

Silica particles with a diameter of 1.0 μm and 2.0 μm were separately suspended in water and deposited onto a glass microscope slide with a micropipette. The solutions dried on the microscope slide leaving near single layers of microspheres. The slide was then inserted into a Vacuum Desk-II Cold Sputter-Etch Unit (Denton Vacuum, Inc., Cherry Hill, NJ) and gold was sputtered onto the slide for 40 and 80 seconds, respectively. Sputtering was performed under vacuum, which allowed the gold to travel in a linear fashion, coating only the top hemisphere of the particles. This creates a material anisotropy, the top hemisphere of the spheres being metallic and the bottom hemispheres being silica.

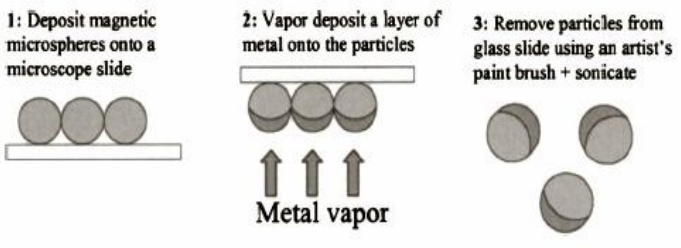

Figure 1. Fabrication process of gold coated polystyrene spheres.

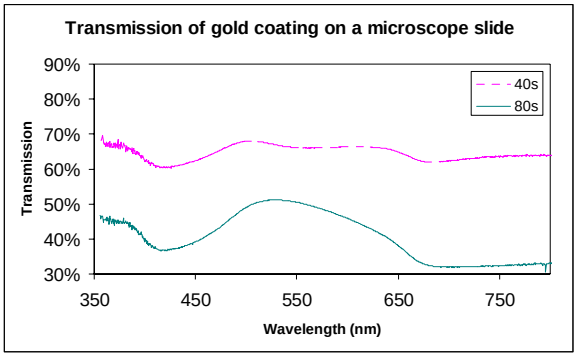

Figure 2. Wavelength dependent attenuation of light caused by the gold coating. The dashed line represents a 40 s duration while the solid line represents an 80 s duration.

The coated particles on the microscope slide have a long shelf life and can be removed from the microscope slide long after they have been coated. We removed the gold coated particles by using an artist's paintbrush. To suspend the coated particles, we sonicated the brush in water for a short amount of time.

3.2. Sample characterization

For our MOONs, in order to find the thickness of gold that corresponds to a specific duration of sputter coating, we used an optical microscope (Olympus IMT-II) interfaced via LabVIEW with a spectrometer (Acton Research Corp., Acton, MA) to measure transmission of bright field light through the gold coated slide. Attenuation caused by the presence of the gold was then determined by dividing the intensity of light transmitted through the coated slide by the intensity of light transmitted through an uncoated region of the same slide (see Figure 2). From this attenuation and given that the skin depth of gold is 17 nm at a wavelength of 589 nm,[44] we calculated that the gold layer was approximately 6.7 ± 0.5 nm for a 40 s coating (dashed line) and 12 ± 1 nm for 80 s (solid line). The error corresponds to the standard deviation estimated by measuring at different points on the gold coated slide. It is worthwhile to note that rough surfaces are not coated as easily as smooth surfaces. So, the actual gold layer thickness on the silica microspheres will most likely be smaller than our calculated value.

Hybrid nanoparticles in solution were dried and characterized using scanning and transmission electron microscopy (SEM, TEM). Examples of silica-silver core-shell particles are shown in Figure 2. So as to not obscure the presence of the gold half-shell, MOONs were *not* coated with an additional metal, as is typical prior to SEM imaging. Enough contrast remained to distinguish the boundary of the gold coating against the silica matrix.

Figure 3. TEM (a, b) and SEM (c, inset) images of 1 micron silica-40 nm silver core-shell particles.

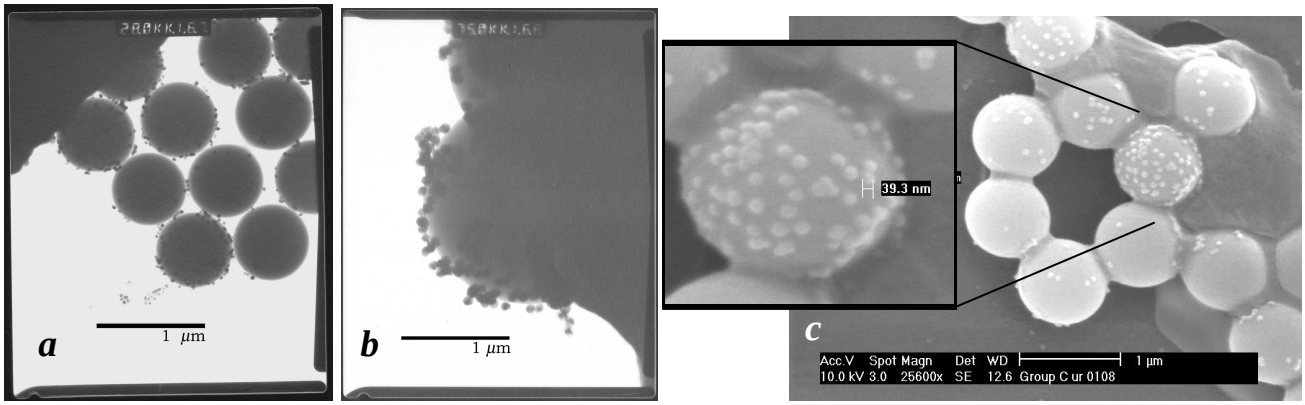

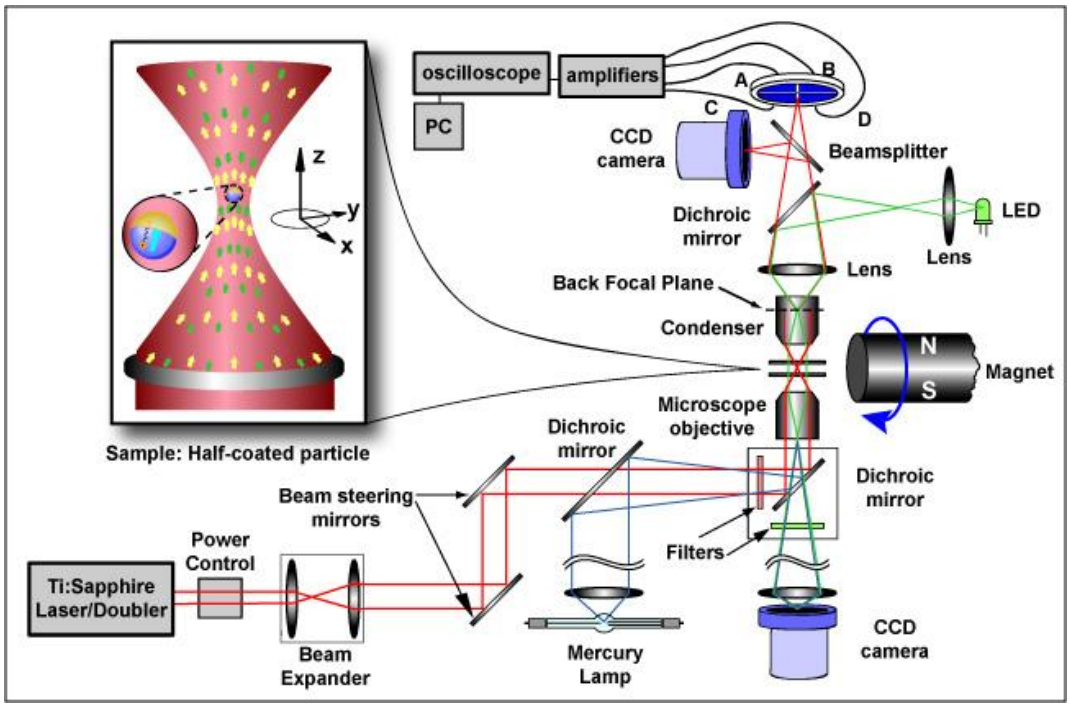

Figure 4. Experimental schematic optical tweezers setup. The apparatus is a conventional system with both reflection and transmission illumination capabilities.

3.3. Experiment

A schematic of the instrumental apparatus is shown in Figure 4. A titanium:sapphire laser system (Tsunami pumped by a Millenia XsJs, Spectra Physics) is used to trap samples. The laser was set to emit continuous-wave near infrared (NIR) radiation at 760 nm, accomplished by reducing the bandwidth enough to inhibit pulsed radiation. The trapping beam then passed through an adjustable neutral density filter wheel to control power. The beam diameter was expanded by a factor of about 4 to just overfill the back aperture of the trapping optics. Beam steering mirrors directed the laser light through a dichroic mirror into a commercial inverted optical microscope (IX71, Olympus). Custom-assembled detection and illumination optics were attached to the microscope above the stage using mechanical rails. Upon entering the microscope, the beam was deflected by a hot mirror. The hot mirror reflects NIR, is partially reflective for ultraviolet light, but transmits visible. The NIR beam was then focused by a 100X (NA = 1.3) oil immersion objective (UPlanFl, Olympus), thus forming the optical trap near the sample plane. Light forward-scattered by the trapped object interfered with the incident laser light and was then recollected by a condenser comprised of another oil immersion objective (PlanApo 60X, NA = 1.4, Olympus). The back focal plane of the condenser was imaged onto a quadrant photodiode (Pacific Silicon Sensor, Inc., Westlake Village, CA) for position detection measurements.[45] Difference voltage signals for the x- and y-axes, as indicated in the inset of Figure 4, and sum voltages from the quadrant diode were amplified and fed into a digitizing oscilloscope (TDS 420, Tektronix) which was interfaced to a computer via LabVIEW. To aid in alignment, light impinging upon the quadrant diode was also split using a non-polarizing beamsplitter and viewed using a ccd camera (Watec). Samples were placed on the translation stage in a chamber consisting of two #0 coverslips separated by double stick tape (~100 μm thick) and sealed with grease to reduce evaporation and convection currents. Two separate regions were formed for a given pair of coverslips, one containing blank silica particles, the other containing hybridized forms of the silica particles (either core-shell or half-shell). Two methods of illumination were possible: (1) transmission from above using an LED of visible wavelength (usually green, max. intensity = 525 nm) and (2) reflection from below using a mercury arc lamp. The sample plane could be imaged in either mode using another ccd camera (CoolSnap) placed on the trinocular tube above the eyepiece of the microscope. Reflection mode was especially helpful by providing more contrast compared to regular bright-field transmission to distinguish metallic coated particles from blank particles near the sample plane. Reflection and fluorescence images of 2 μm and 3.4 μm MOONs, respectively, undergoing Brownian motion are shown in Figure 5.

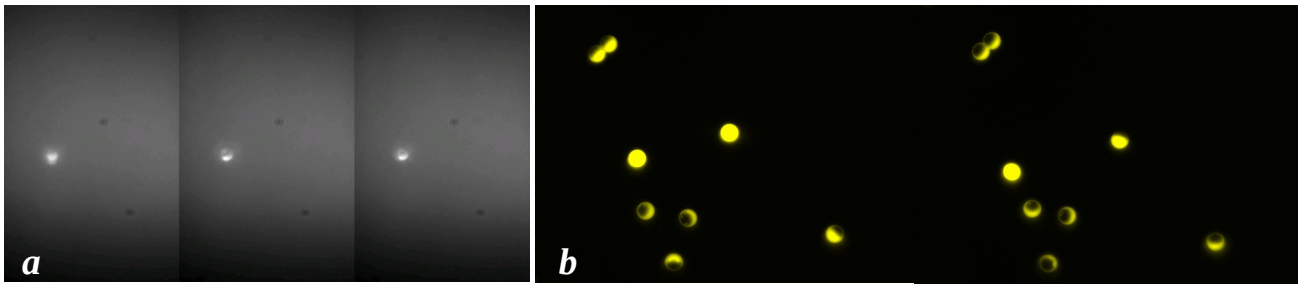

Figure 5. (a) 2 μm MOdulated Optical Nanoprobe (MOON) undergoing Brownian motion in reflection mode. The time between images is approximately 0.3 s (b) 3.4 μm MOONs in epifluorescence. Time between images is seconds.

Core-shell hybrid particles were trapped in water approximately 10 μm above the bottom coverslip and their position fluctuations in time were recorded. Each particle was held for several seconds to ensure stable laser tweezing before the time trace was started. To make certain we were operating in the linear regime, 5-10 particles were trapped at approximately 8-10 different laser beam powers. Half-shell particles could not be stably trapped using our single-beam gradient optical tweezers; nevertheless, position trajectories were imaged and recorded.

4. DATA ANALYSIS

The following data analysis procedure was performed at a series of laser powers for each particle type. Quadrant diode voltage fluctuation time traces were acquired in three channels: two difference voltage traces for the radial dimensions (x and y), and one sum voltage trace for all diodes. For each radial dimension, a histogram of the voltages was recorded to ensure a Boltzmann distribution. Note, a Boltzmann distribution is expected for position; however, if the particle is close to the trap center, the relationship between position and voltage can be assumed linear.[4] Curves that exhibited behavior that deviated from a Boltzmann distribution were discarded.

The x- and y-dimension curves were both normalized by dividing by the sum voltage trace. For each radial dimension, the power spectral density (PSD) estimate was calculated using the "periodogram" function of MATLAB. The resulting PSD's were averaged, and the final mean PSD was binned logarithmically in frequency, a noise reduction technique otherwise known as "blocking".[40,41] Using least squares curve-fitting, a Lorentzian profile was fit to each PSD curve according to Eq. (2). To avoid effects due to low frequency errors from beam pointing fluctuations and high frequency errors from detector response[40,41] or aliasing,[46] only points with abscissa between 10^1 Hz and about half the Nyquist frequency were used in the fit. Fit parameters were the corner frequency, in Hz, and the PSD amplitude S_0, in units V^2/Hz. S_0 can be converted to nm^2/Hz after calibrating volts to nanometers, either by inducing a known spatial

Figure 6. Typical voltage fluctuation time traces. Channels 1, 2 and 3 are the x-difference, y-difference and sum voltages, respectively

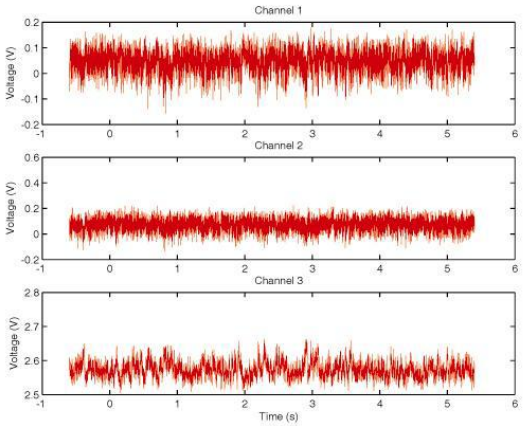

Figure 7. Histograms of visited voltages. For particles close to the trap focus, the voltage, which is proportional to position, is Boltzmann distributed.

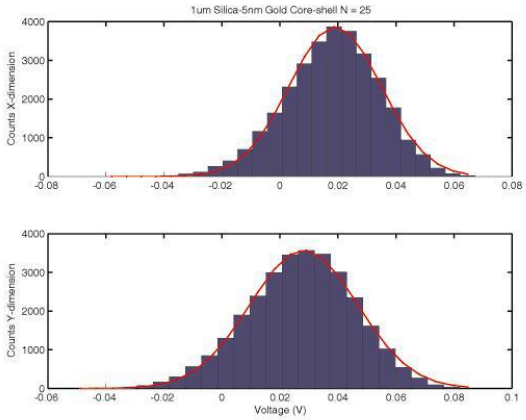

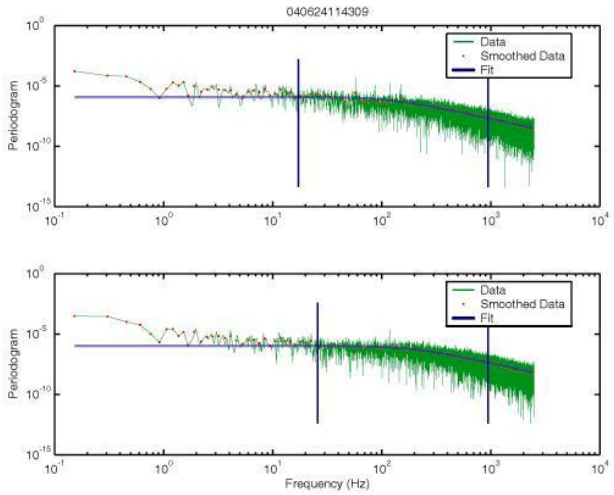

Figure 8. Individual x- and y- dimension PSD's for a 1 μm silica-5 nm gold core-shell particle (thin line). A Lorentzian profile (thick line) is fit to the logarithmically binned data (red dots). .

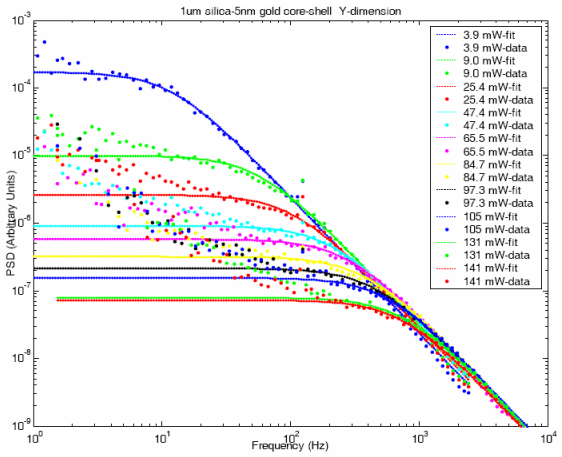

Figure 9. PSD as a function of laser beam power. Low frequency noise from beam point fluctuations is evident.

displacement of the particle and measuring the voltage, by estimating the rms displacement from the voltage histograms, or by assuming the Stoke's force is in equilibrium with the optical restoring force.[39] The corner frequency is related to trap stiffness by a proportionality constant assuming the solvent viscosity is constant.

Because half-coated particles could not be stably trapped, image video recordings were acquired, analyzed qualitatively and compared to phenomena in previous literature.

5. RESULTS

Figure 6 shows typical voltage fluctuation time trace curves. The particular data shown represents a 1 μm silica-5 nm gold core-shell trapped by . Figure 7 indicates a histogram of the voltage time traces from Figure 6. Since the positions visited by the particle are Gaussian distributed in accordance with Eq. (4), the assumption that the voltage-position relationship is linear for trapped particles is justified. There appears to be a slight shift of the trap center as well as a small amount of asymmetry. This is probably caused by minor misalignment and detector crosstalk between radial directions. After normalization, the PSD's are calculated for each dimension. The original PSD, the blocked PSD, and the Lorentzian fit are plotted on the same graph in Figure 8. This procedure was done for each particle at a series of laser powers ranging from 1-150 mW entering the trapping objective. All PSD's and fits for this particle type are plotted in Figure 9. To better determine if these powers are low enough to remain in the linear regime, we can look at the dependence of corner frequency on power for each particle type in Figures 10a-f. For each plot of Figure 10, we see two regions: a low power regime with a lower f_c/power (slope) and a high power regime with higher f_c/power (steeper slope). This can be explained by considering decreased solvent viscosity due to increased heat absorption at high laser powers. Since, however, this effect is not markedly increased when comparing blank particles to metal-containing particles, several conclusions can be made. One possibility is that the metal colloids are truly too small to provide much more than a small perturbation. In this case, heat absorption is mostly due to the solvent and the silica. In addition, the metal shell does not hinder the optical trap to any measurable degree. This is clear from Table 1 in which the corner frequency per power is tabulated at high and low power for each particle type. There is no appreciable difference in trap stiffness between blank silica, aminated silica, and silica with 5 nm colloid shells. A slight drop in trap stiffness occurs for 40 nm colloid shells – this may be signaling the onset of limited trapping stability due to the increased scattering and reflection from the metal colloids. If the colloid presence has a small effect, trapping of hybrid nanoparticle probes will have the same behavior as simpler homogeneous nanoparticles - a desirable outcome when sensing is most significant. This suggests, however, that no enhancement has occurred due to increased polarizability.

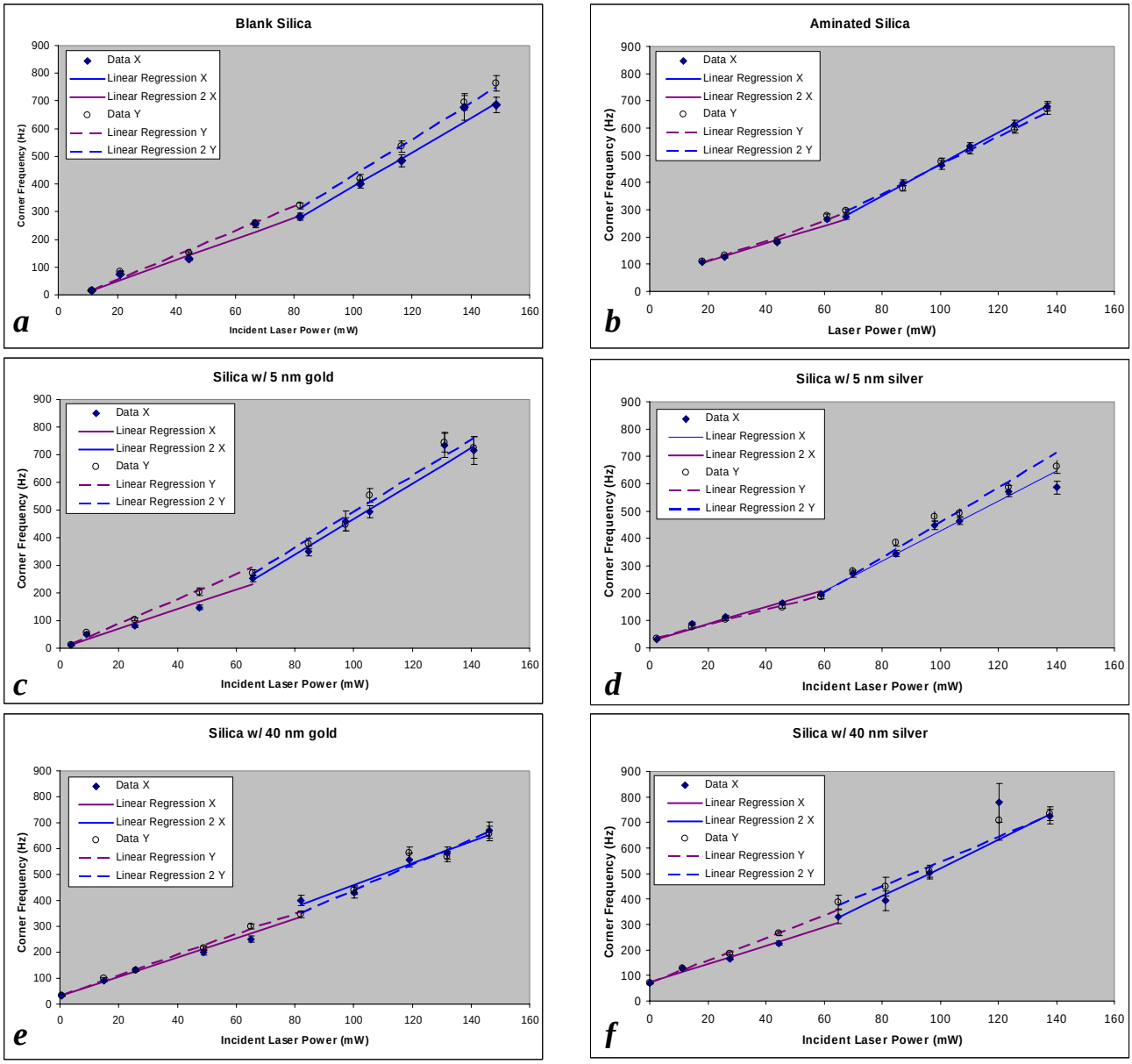

Figure 10. (a-f) Corner frequency dependence on laser beam power. In all plots two regimes are evident: a low power region with lower f_c/power and a high power region with higher f_c/power. The larger slope is attributed to increased solvent viscosity with increased heat absorption. No significant difference is apparent between blank particles and coated particles., nor between particles with 5 nm shells and particles with 40 nm shells.

Another more likely possibility is that few colloids actually remained on the silica cores. Particle uniformity is a nontrivial issue in the fabrication of nanoparticles. The distribution of colloid coverage on silica cores is likely to be large in our samples. Thus, trapping events between different particles may not be comparable. This is also true of our half-shell particles. Coating thickness can vary drastically from particle to particle within a single sample.

For our silica-gold core-half-shell particles, or MOONs, no three-dimensionally stable trapping was observed. Most particles that diffused below the trap were quickly confined radially but were then forced upwards by the axial scattering force. In several extraordinary, yet repeatable cases a MOON would remain in the lower cone of the laser beam below the focus. The particle would undergo fast rotations about the optical axis while continuously being bumped by random fluctuations in all directions. If the trap location were slowly moved relative to the surrounding medium, the particle

f_c/Power	X-dimension		Y-dimension	
Particle	*Low Power*	*High Power*	*Low Power*	*High Power*
Silica	3.83±0.09	6.17±0.39	4.44±0.08	6.54±0.35
Silica-amine	3.25±0.15	5.83±0.27	3.66±0.12	5.26±0.20
Silica-am-5nm gold	3.54±0.12	6.41±0.42	4.52±0.14	6.52±0.37
Silica-am-5nm silver	3.08±0.09	5.48±0.19	2.71±.08	6.39±0.20
Silica-am-40nm gold	3.74±0.11	4.18±0.47	3.95±0.09	4.90±0.37
Silica-am-40nm silver	3.60±0.16	5.54±0.59	4.39±0.14	4.87±0.51

Table 1. Summary of corner frequency per power measurements for silica-gold core-shell nanoparticles.

would continue its clockwise circular trajectory about the beam focus, verifying that it was truly loosely confined to the lower cone of the laser beam. Similar rotational behavior has been described using Laguerre-Gaussian beams.[46]

6. CONCLUSIONS AND FUTURE WORK

We have optically manipulated hybrid nanoparticle systems comprised of silica-gold and silica-silver. Our analysis of trap stiffness measurements reveals several possibilities. The trapping of core-shell hybrid systems fabricated using spatially separated colloids for shells is possible. Redistribution of the colloids such that the shell covers approximately half of the core induces a strong asymmetry in the particle that strongly hinders conventional, stable, three-dimensional optical trapping, but it may offer schemes for yet unstudied rotational phenomena.

Several improvements must be made before conclusive data can be acquired. Trapping force-constant analysis techniques must take into account all sources of error present in practical measurements, including unintentional filtering due to detection equipment, aliasing from digital recording equipment, and viscosity changes due to surface proximity and heat absorption. Another aspect of concern is the design of a fabrication method that can provide more uniform distributions of the same hybrid particle. Our MOON fabrication scheme requires the creation of a monolayer of core particles such that there are few defects. Defects in the monolayer can cause too few cores to get coated and many to be uncoated, or they can enable the presence of coating material to be present without cores. Work is currently underway to establish a wide-area low-defect monolayer and to half-coat more precisely particles using molecular beam epitaxy.

ACKNOWLEDGEMENTS

We acknowledge National Science Foundation grant DMR 9900434, National Institutes of Health grant 8RO1 EB000250-09, and DARPA F49620-03-1-0297 for support.

REFERENCES

1. J. E. Molloy and M. J. Padgett, "Lights, action: optical tweezers," *Contemp. Phys.*, **43**, 241-258 (2002).
2. J. E. Molloy, K. Dholakia, and M. J. Padgett, "Preface: Optical tweezers in a new light," *J. Mod. Opt.*, **50**, 1501-1507 (2003).
3. D. G. Grier, "A revolution in optical manipulation," *Nature*, **424**, 810-816 (2003).
4. U. Bockelmann, "Single-molecule manipulation of nucleic acids," *Curr. Opin. Struct. Biol.*, **14**, 368-373 (2004).
5. K. Sasaki, M. Koshioka, H. Misawa, N. Kitamura, and H. Masuhara, "Pattern-Formation and Flow-Control of Fine Particles by Laser-Scanning Micromanipulation," *Opt. Lett.*, **16**, 1463-1465 (1991).
6. H. M. Warrick, R. M. Simmons, J. T. Finer, T. Q. P. Uyeda, S. Chu, and J. A. Spudich, "In-Vitro Methods for Measuring Force and Velocity of the Actin-Myosin Interaction Using Purified Proteins," **39**, 1-21 (1993).
7. E. R. Dufresne and D. G. Grier, "Optical tweezer arrays and optical substrates created with diffractive optics," *Rev.*

Sci. Instrum., **69**, 1974-1977 (1998).
8. J. Liesener, M. Reicherter, T. Haist, and H. J. Tiziani, "Multi-functional optical tweezers using computer-generated holograms," *Opt. Commun.*, **185**, 77-82 (2000).
9. A. Ashkin and J. M. Dziedzic, "Observation of Light-Scattering from Nonspherical Particles Using Optical Levitation," *Appl. Optics*, **19**, 660-668 (1980).
10. P. Galajda and P. Ormos, "Complex micromachines produced and driven by light," *Appl. Phys. Lett.*, **78**, 249-251 (2001).
11. P. Viravathana and D. W. M. Marr, "Optical trapping of titania/silica core-shell colloidal particles," *J. Colloid Interface Sci.*, **221**, 301-307 (2000).
12. W. E. Doering and S. M. Nie, "Spectroscopic tags using dye-embedded nanoparticles and surface-enhanced Raman scattering," *Anal. Chem.*, **75**, 6171-6176 (2003).
13. X. H. Gao and S. M. Nie, "Quantum dot-encoded mesoporous beads with high brightness and uniformity: Rapid readout using flow cytometry," *Anal. Chem.*, **76**, 2406-2410 (2004).
14. H. Furukawa and I. Yamaguchi, "Optical trapping of metallic particles by a fixed Gaussian beam," *Opt. Lett.*, **23**, 216-218 (1998).
15. J. R. Arias-Gonzalez and M. Nieto-Vesperinas, "Optical forces on small particles: attractive and repulsive nature and plasmon-resonance conditions," *J. Opt. Soc. Am. A-Opt. Image Sci. Vis.*, **20**, 1201-1209 (2003).
16. J. Prikulis, F. Svedberg, M. Kall, J. Enger, K. Ramser, M. Goksor, and D. Hanstorp, "Optical spectroscopy of single trapped metal nanoparticles in solution," *Nano Lett.*, **4**, 115-118 (2004).
17. F. Yan, H. Xu, J. Anker, R. Kopelman, B. Ross, A. Rehemtulla, and R. Reddy, "Synthesis and characterization of silica-embedded iron oxide nanoparticles for magnetic resonance imaging," *J. Nanosci. Nanotechnol.*, **4**, 72-76 (2004).
18. S. M. Buck, H. Xu, M. Brasuel, M. A. Philbert, and R. Kopelman, "Nanoscale probes encapsulated by biologically localized embedding (PEBBLEs) for ion sensing and imaging in live cells," *Talanta*, **63**, 41-59 (2004).
19. S. L. R. Barker, R. Kopelman, T. E. Meyer, and M. A. Cusanovich, "Fiber-optic nitric oxide-selective biosensors and nanosensors," *Anal. Chem.*, **70**, 971-976 (1998).
20. S. L. R. Barker and R. Kopelman, "Development and cellular applications of fiber optic nitric oxide sensors based on a gold-adsorbed fluorophore," *Anal. Chem.*, **70**, 4902-4906 (1998).
21. S. L. R. Barker, H. A. Clark, S. F. Swallen, R. Kopelman, A. W. Tsang, and J. A. Swanson, "Ratiometric and fluorescence lifetime-based biosensors incorporating cytochrome c ' and the detection of extra- and intracellular macrophage nitric oxide," *Anal. Chem.*, **71**, 1767-1772 (1999).
22. C. J. Behrend, J. N. Anker, and R. Kopelman, "Brownian modulated optical nanoprobes," *Appl. Phys. Lett.*, **84**, 154-156 (2004).
23. C. J. Behrend, J. N. Anker, B. H. McNaughton, M. Brasuel, M. A. Philbert, and R. Kopelman, "Metal-capped Brownian and magnetically modulated optical nanoprobes (MOONs): Micromechanics in chemical and biological microenvironments," *J. Phys. Chem. B*, **108**, 10408-10414 (2004).
24. A. Ashkin and J. P. Gordon, "Stability of radiation-pressure particle traps: an optical Earnshaw theorem," **8**, 511-513 (1983).
25. R. R. Agayan, F. Gittes, R. Kopelman, and C. F. Schmidt, "Optical trapping near resonance absorption," *Appl. Optics*, **41**, 2318-2327 (2002).
26. J. D. Jackson, *Classical Electrodynamics*, 3rd ed. (John Wiley & Sons, Inc., New York, 1999),
27. Y. Harada and T. Asakura, "Radiation Forces on a Dielectric Sphere in the Rayleigh Scattering Regime," *Opt. Commun.*, **124**, 529-541 (1996).
28. J. P. Gordon, "Radiation Forces and Momenta in Dielectric Media," *Phys. Rev. A*, **8**, 14-21 (1973).
29. A. Ashkin, J. M. Dziedzic, J. E. Bjorkholm, and S. Chu, "Observation of a Single-Beam Gradient Force Optical Trap for Dielectric Particles," *Opt. Lett.*, **11**, 288-290 (1986).
30. K. Svoboda and S. M. Block, "Optical Trapping of Metallic Rayleigh Particles," *Opt. Lett.*, **19**, 930-932 (1994).
31. A. Ashkin, "Forces of a Single-Beam Gradient Laser Trap on a Dielectric Sphere in the Ray Optics Regime," *Biophys. J.*, **61**, 569-582 (1992).
32. R. M. Simmons, J. T. Finer, S. Chu, and J. A. Spudich, "Quantitative measurements of force and displacement using

an optical trap," *Biophys. J.*, **70**, 1813-1822 (1996).
33. W. Singer, S. Bernet, N. Hecker, and M. Ritsch-Marte, "Three-dimensional force calibration of optical tweezers," *J. Mod. Opt.*, **47**, 2921-2931 (2000).
34. L. P. Ghislain, N. A. Switz, and W. W. Webb, "Measurement of Small Forces Using an Optical Trap," *Rev. Sci. Instrum.*, **65**, 2762-2768 (1994).
35. H. Felgner, O. Muller, and M. Schliwa, "Calibration of Light Forces in Optical Tweezers," *Appl. Optics*, **34**, 977-982 (1995).
36. N. Malagnino, G. Pesce, A. Sasso, and E. Arimondo, "Measurements of trapping efficiency and stiffness in optical tweezers," *Opt. Commun.*, **214**, 15-24 (2002).
37. F. Gittes and C. F. Schmidt, "Thermal Noise Limitations on Micromechanical Experiments," *Eur. Biophys. J. Biophys. Lett.*, **27**, 75-81 (1998).
38. K. Berg-Sorensen and H. Flyvbjerg, "Power spectrum analysis for optical tweezers," *Rev. Sci. Instrum.*, **75**, 594-612 (2004).
39. A. Buosciolo, G. Pesce, and A. Sasso, "New calibration method for position detector for simultaneous measurements of force constants and local viscosity in optical tweezers," *Opt. Commun.*, **230**, 357-368 (2004).
40. K. Berg-Sorensen, L. Oddershede, E. L. Florin, and H. Flyvbjerg, "Unintended filtering in a typical photodiode detection system for optical tweezers," *J. Appl. Phys.*, **93**, 3167-3176 (2003).
41. I. M. Tolic-Norrelykke, K. Berg-Sorensen, and H. Flyvbjerg, "MatLab program for precision calibration of optical tweezers," *Comput. Phys. Commun.*, **159**, 225-240 (2004).
42. F. Osterloh, H. Hiramatsu, R. Porter, and T. Guo, "Alkanethiol-induced structural rearrangements in silica-gold core-shell-type nanoparticle clusters: An opportunity for chemical sensor engineering," *Langmuir*, **20**, 5553-5558 (2004).
43. Y. A. Sun and Y. N. Xia, "Triangular nanoplates of silver: Synthesis, characterization, and use as sacrificial templates for generating triangular nanorings of gold," *Adv. Mater.*, **15**, 695-699 (2003).
44. M. Born and E. Wolf, "Principles of Optics," 6th ed., Ch. 13 (Cambridge University Press, New York, NY, 1980).
45. F. Gittes and C. F. Schmidt, "Interference model for back-focal-plane displacement detection in optical tweezers," *Opt. Lett.*, **23**, 7-9 (1998).
46. W. H. Press, S. A. Teulosky, W. T. Vetterling, and B. P. Flannery, "Numerical Recipes in C," 2nd ed., 501, 576 (Cambridge University Press, Cambridge, MA, 1992).
47. A. T. O'Neil and M. J. Padgett, "Three-dimensional optical confinement of micron-sized metal particles and the decoupling of the spin and orbital angular momentum within an optical spanner," *Opt. Commun.*, **185**, 139-143 (2000).